molecules

MDPI

Article

A Zn(II) Coordination Polymer for Fluorescent Turn-Off Selective Sensing of Heavy Metal Cation and Toxic Inorganic Anions

Yaxin Li, Mouyi Zhang, Ying Wang, Lei Guan *, Di Zhao, Xinyu Hao and Yuting Guo

School of Petrochemical Engineering, Liaoning Petrochemical University, Fushun 113001, China
* Correspondence: guanlei@lnpu.edu.cn

Abstract: A novel coordination polymer $[Zn(atyha)_2]_n$ (**1**) (Hatyha = 2-(2-aminothiazole-4-yl)-2- hydroxyiminoacetic acid) was constructed by hydrothermal reaction of Zn^{2+} with Hatyha ligand. CP **1** exhibits a 2D (4,4)-connected topological framework with Schläfli symbol of $\{4^4 \cdot 6^2\}$, where atyha$^-$ anions serve as tridentate ligands, bridging with Zn^{2+} through carboxylate, thiazole and oxime groups. CP **1** displays a strong ligand-based photoluminescence at 390 nm in the solid state, and remains significantly structurally stable in water. Interestingly, it can be utilized as a fluorescent probe for selective and sensitive sensing of Fe^{3+}, $Cr_2O_7^{2-}$ and MnO_4^- through the fluorescent turn-off effect with limit of detection (LOD) of 3.66×10^{-6}, 2.38×10^{-5} and 2.94×10^{-6} M, respectively. Moreover, the efficient recyclability for detection of Fe^{3+} and $Cr_2O_7^{2-}$ is better than that for MnO_4^-. The mechanisms of fluorescent quenching involve reversible overlap of UV-Vis absorption bands of the analytes (Fe^{3+}, $Cr_2O_7^{2-}$ and MnO_4^-) with fluorescence excitation and emission bands for CP **1**, respectively.

Keywords: coordination polymer; fluorescent; selective sensing; metal cation; inorganic anion

Citation: Li, Y.; Zhang, M.; Wang, Y.; Guan, L.; Zhao, D.; Hao, X.; Guo, Y. A Zn(II) Coordination Polymer for Fluorescent Turn-Off Selective Sensing of Heavy Metal Cation and Toxic Inorganic Anions. *Molecules* **2024**, *29*, 2943. https://doi.org/10.3390/molecules29122943

Academic Editor: Shengjie Wang

Received: 28 May 2024
Revised: 15 June 2024
Accepted: 18 June 2024
Published: 20 June 2024

1. Introduction

Nowadays, coordination polymers (CPs), as one class of promising functional materials, have received widespread attention not only due to unique topologies, such as multiple active sites, modifiable channels and fascinating architectures, but also due to excellent performance and potential applications in various fields, such as catalyst carrier, proton conducting, sensing, magnetic and fluorescent materials, gas separation and storage [1–8]. In particular, the structural diversity and multi-functional characteristics of CPs aroused intense interest in the design and construction of chemical sensing materials [9–12]. It has been well documented that due to their fast response, high sensitivity and naked eye monitoring, fluorescent CPs can be one type of good chemical sensor for detecting analytes through fluorescence quenching, enhancement or shift [13–16]. Reasonable selection of metal nodes and organic linkers is of great significance for the construction of fluorescent CPs [17–19]. It was found that fluorescent CPs constructed by heterocyclic carboxylate ligands and d^{10} metal centers show excellent photoluminescence performance [20,21].

Recently, the rapid development of industry has led to inevitable increases in the discharge of hazardous species into the water environment, including heavy metal ions, inorganic oxo-anions and other industrial pollutants. Improper treating and failure to detect these pollutants in time may pose a threat to the ecosystem and cause various human diseases [22]. Fe^{3+} plays an important role in metabolic processes of the human body and is one of the indispensable substances in the uptake of oxygen through blood in the body and in the formation of DNA and RNA. Excess or deficiency of Fe^{3+} in the body can result in serious diseases, such as hereditary hemochromatosis and endotoxemia [23]. Inorganic oxo-anions, especially $Cr_2O_7^{2-}$ and MnO_4^-, have been considered as highly toxic pollutants originating from industrial wastewater, and may cause skin allergies or

even induce cancers [24]. Therefore, it is imperative to exploit fluorescent CPs to efficiently detect these hazardous species in aqueous media.

In this work, Hatyha ligand was selected to construct a CP based on three structural characteristics: (a) it contains Lewis basic N sites, which can coordinate with Zn(II); (b) it features carboxylate and oxime groups that may adopt various coordination modes to construct complicated topology; (c) it has N, O donors and acceptors, which can form hydrogen bonds and generate high-dimensional supramolecular structures. We have carried out the coordination reaction of atyha$^-$ ligand with Zn(II) under hydrothermal condition to successfully synthesize a fluorescent CP $[Zn(atyha)_2]_n$ (**1**). CP **1** features an infinite 2D-layered structure, displaying strong luminescence emission in solid state at room temperature. It was found that the fluorescence intensity of CP **1** could be markedly quenched by Fe^{3+}, $Cr_2O_7^{2-}$ and MnO_4^- in the presence of interfering ions, respectively. CP **1** can behave as a chemical sensor based on the fluorescence turn-off effect, with the characteristics of selective and sensitive detection. Furthermore, it also has a relatively low LODs of 3.66×10^{-6}, 2.38×10^{-5} and 2.94×10^{-6} M for Fe^{3+}, $Cr_2O_7^{2-}$ and MnO_4^-, respectively.

2. Results and Discussion

2.1. Crystal Structure of CP **1**

Single crystal X-ray diffraction analysis reveals that CP **1** crystallizes in the orthorhombic unit cell with space group *Pbcn* (Table 1). The asymmetric unit consists of one Zn center and two atyha$^-$ ligands (Figure 1a), with the chemical formula of $[Zn(atyha)_2]_n$. Each Zn atom is six-coordinated by two thiazole N atoms and two oxime N atoms from two atyha$^-$ ligands and two carboxylate O atoms of two atyha$^-$ ligands, showing a distorted ZnN_4O_2 octahedral geometry (Figure 1b). The Zn-N distances are between 2.169(2) Å and 2.050(2) Å, the Zn-O lengths are 2.2504(17) Å, the O-Zn-N and N-Zn-N bond angles are in the ranges of 83.84(8)°–162.22(8)° and 76.20(9)°–169.18(13)° (Table 2), respectively, which are similar to the values reported in the references for other Zn complexes [25]. The atyha$^-$ ligand adopts the carboxylate group to bind to Zn center in a monodentate coordination fashion, as well as thiazole N atom and oxime N atom chelation with Zn center, while the amino group remains uncoordinated. The atyha$^-$ anions are employed as tridentate ligands to link with adjacent Zn centers, generating a 2D-layered architecture through carboxylate, thiazole and oxime groups (Figure 1c). The hydrogen bonds formed between the amino N atom and the carboxylate O atom (N1-H1B···O2^{ii}) can expand the layered structure into a 3D supramolecular structure (Figure 1d). The hydrogen bonds are formed between oxime O atoms and carboxylate O atoms (O3-H3···O2), and between amino N atoms and carboxylate O atoms (N1-H1A···O1^{i} and N1-H1A···O2) (Table S1), which make the structure more stable.

Table 1. Crystallographic data and structure refinement details for CP **1**.

	1
Chemical formula	$C_{10}H_8N_6O_6S_2Zn$
M_r	437.71
Crystal system,	Orthorhombic
Space group	*Pbcn*
Temperature(K)	253
a, *b*, *c* (Å)	11.6451(16), 7.2951(8), 16.761(2)
Z	4
V (Å^3)	1423.9(3)
μ (mm^{-1})	2.07
No. of measured, independent and obverted [$I > 2\sigma(I)$] reflection	32,248, 1631, 1500
R_{int}	0.057
$(\sin\theta/\lambda)_{max}$ (Å^{-1})	0.650

Table 1. *Cont.*

	1
$R[F^2 > 2\sigma(F^2)]$, $\omega R(F^2)$, S	0.035, 0.098, 1.08
No. of reflections	1631
No. of parameters	115
No. of restraints	1
R_1, ωR_2 $[I \geq 2\sigma(I)]$	0.0349, 0.0956
R_1, ωR_2 (all data)	0.0378, 0.0978
$\Delta\rho_{max}$, $\Delta\rho_{min}$ (e·Å^{-3})	1.63, −1.37

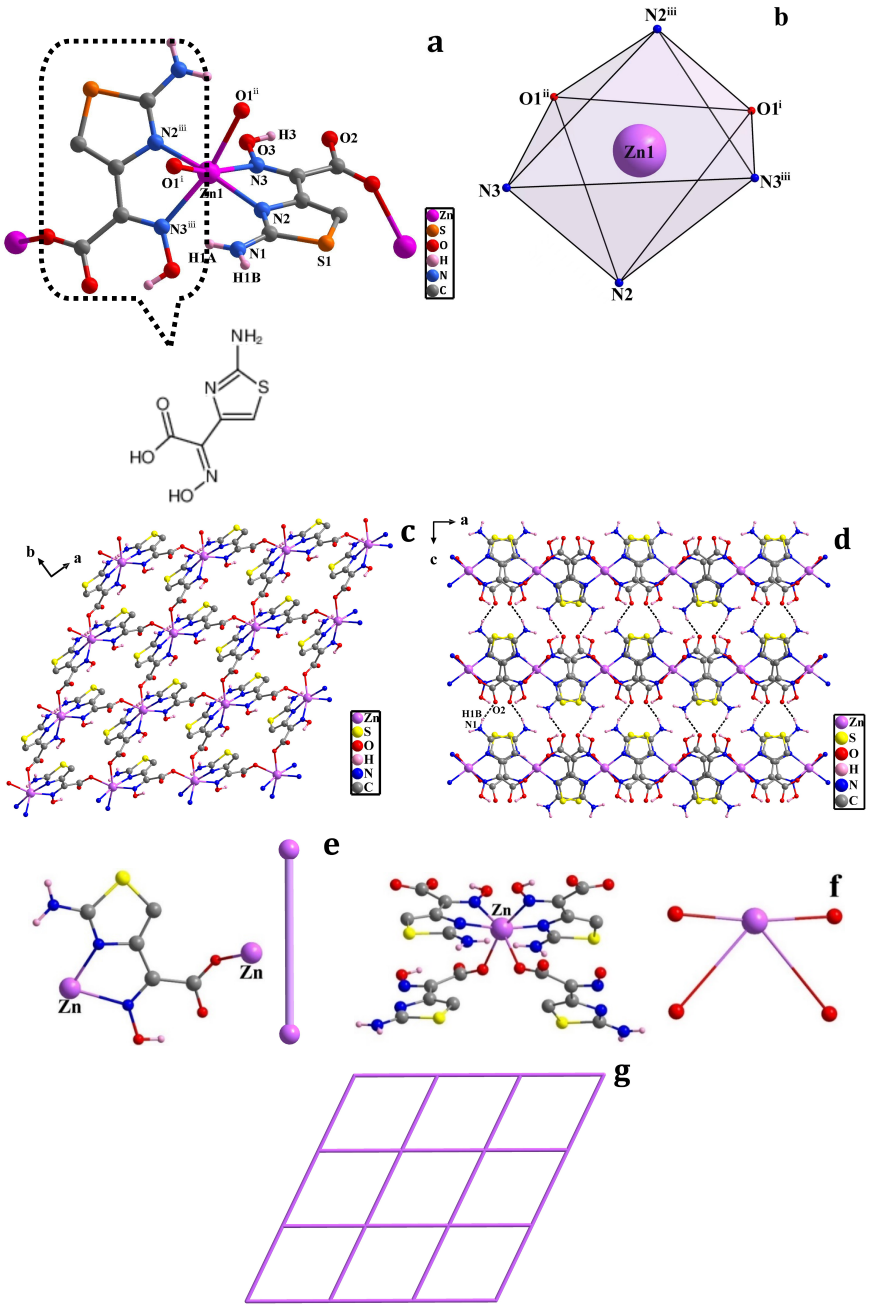

Figure 1. (**a**) A drawing showing the coordination environment about Zn^{2+}; (**b**) octahedral coordination configuration of Zn^{2+}; (**c**) 2D-layered structure; (**d**) 3D supramolecular structure; (**e**) bridged atyha$^-$ ligand-based node; (**f**) 4-c node of Zn^{2+}; (**g**) topological structure.

Table 2. Selected bond lengths (Å) and angles (°) for CP **1**.

Atom1-Atom2	Distance	Atom1-Atom2	Distance	Atom1-Atom2	Distance
Zn1-O1^{i}	2.2504(17)	Zn1-N2	2.050(2)	Zn1-N3	2.169(2)
Zn1-O1^{ii}	2.2504(17)	Zn1-N2^{iii}	2.050(2)	Zn1-N3^{iii}	2.169(2)
Atom1-Atom2-Atom3	**Angle**	**Atom1-Atom2-Atom3**	**Angle**	**Atom1-Atom2-Atom3**	**Angle**
O1^{i}-Zn1-O1^{ii}	79.32(7)	N2^{iii}-Zn1-N2	169.18(13)	N3^{iii}-Zn1-O1^{ii}	162.22(8)
N2-Zn1-O1^{ii}	90.24(8)	N2-Zn1-N3	76.20(9)	N3-Zn1-O1^{i}	162.22(8)
N2^{iii}-Zn1-O1^{i}	90.24(8)	N2^{iii}-Zn1-N3	97.77(9)	N3-Zn1-O1^{ii}	83.84(8)
N2^{iii}-Zn1-O1^{ii}	98.10(8)	N2^{iii}-Zn1-N3^{iii}	76.20(9)	N3^{iii}-Zn1-O1i	83.84(8)
N2-Zn1-O1^{i}	98.10(8)	N2-Zn1-N3^{iii}	97.77(9)	N3^{iii}-Zn1-N3	113.44(14)

Symmetry codes: (i) x+1/2, y+1/2, −z+3/2; (ii) − x+1/2, y+1/2, z; (iii) −x+1, y, −z+3/2.

From a topological perspective, each atyha^{-} ligand coordinates with two Zn centers, which can be considered as a bridging ligand-based node (Figure 1e). Each Zn center is surrounded by four atyha^{-} ligands, which can be regarded as a 4-c node (Figure 1f). Therefore, CP **1** features a 4, 4-c network structure with a Schläfli symbol of $\{4^4 \cdot 6^2\}$ (Figure 1g) [26].

2.2. TG Analysis

The TG analysis was performed to investigate the thermal stability of CP **1** (Figure S1). The framework of CP **1** can remain stable before the temperature reaches 196 °C. As the temperature continues to rise, the framework structure of CP **1** undergoes structural collapse and thermal decomposition at 290 °C, resulting in abrupt weight loss, and then it tends to slow down, due to the disintegration of atyha^{-} ligand. At 900 °C, CP **1** has not fully decomposed, and the TGA curve still follows a downward trend. The residue may be a mixture of ZnO and ZnS.

*2.3. PXRD of CP **1***

The powder X-ray diffraction (PXRD) measurement was carried out to confirm the bulk phase purity of CP **1** (Figure S2). The measured pattern of CP **1** was in agreement with the simulated one generated from single crystal X-ray diffraction, revealing that the obtained bulk samples were pure phase. The sample powder of CP **1** was immersed in deionized water for 12 hours and 7 days, respectively, and after centrifugation and natural drying, the PXRD analyses were performed (Figure S3). The results revealed that the experimental patterns of the soaked samples were consistent with the simulated one, manifesting that the framework of CP **1** was intact and possessed high stability in water.

2.4. Fluorescence Spectrum

The solid-state luminescent spectra of CP **1** and free Hatyha ligand were investigated at room temperature (Figure 2). The free Hatyha ligand demonstrates the maximum emission centered at 382 nm when excited at 282 nm. The band may be originated from $\pi \rightarrow \pi^*$ and/or $n \rightarrow \pi^*$ transitions [27]. The luminescent band of CP **1** displays maximum emission at 390 nm (λ_{ex} = 292 nm). Considering the d^{10} electron configuration of Zn(II), it is difficult to be oxidized or reduced. Therefore, the emission may result from neither ligand-to-metal charge transfer nor metal-to-ligand charge transfer, but the fluorescence emission of CP **1** can be attributed to intraligand $\pi \rightarrow \pi^*$ and/or $n \rightarrow \pi^*$ charge transfer [27]. In addition, the emission band of CP **1** indicates red-shift of 8 nm in comparison with those of free Hatyha ligand. This perturbation may result from the coordination interactions of atyha^{-} ligands with central metal ions.

2.5. Selective Sensing of Fe^{3+}

Considering the excellent fluorescent property and water stability of CP **1**, it can be utilized as a fluorescent sensor. From the perspective of environmental protection, water can be used as the medium; moreover, the aqueous suspension of CP **1** shows strong fluorescence intensity. Therefore, the powder sample of CP **1** was ultrasonically dispersed

in water as a blank sample to investigate its fluorescent sensing behaviors toward different metal ions. Upon addition of MCl_x solutions (M = Na^+, Mg^{2+}, Ba^{2+}, Sr^{2+}, Mn^{2+}, Zn^{2+}, Ca^{2+}, K^+, Cd^{2+}, Pb^{2+}, Al^{3+}, Cr^{3+}, Co^{2+}, Cu^{2+}, Ni^{2+}, Fe^{3+}) to the aqueous suspensions of CP **1** (0.5×10^{-5} M) with metal ion concentration of 0.01 M in the mixture, the emission spectra of the suspensions were measured at the excitation wavelength of 334 nm (Figure 3a). In comparation with the blank sample, Na^+ can cause fluorescence enhancement of CP **1;** nevertheless, the addition of other metal ions can lead to significant decreases in the fluorescence intensities of CP **1**, especially Fe^{3+} with quenching efficiency of 99.5%, indicating that CP **1** possesses efficient fluorescent turn-off sensing of Fe^{3+} (Figure 3b).

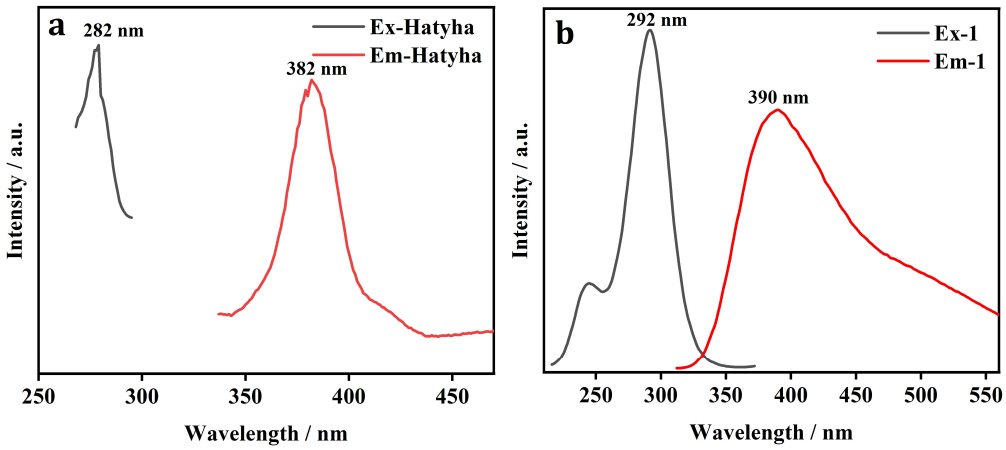

Figure 2. Fluorescence excitation and emission spectra of (**a**) free Hatyha ligand and (**b**) CP **1**.

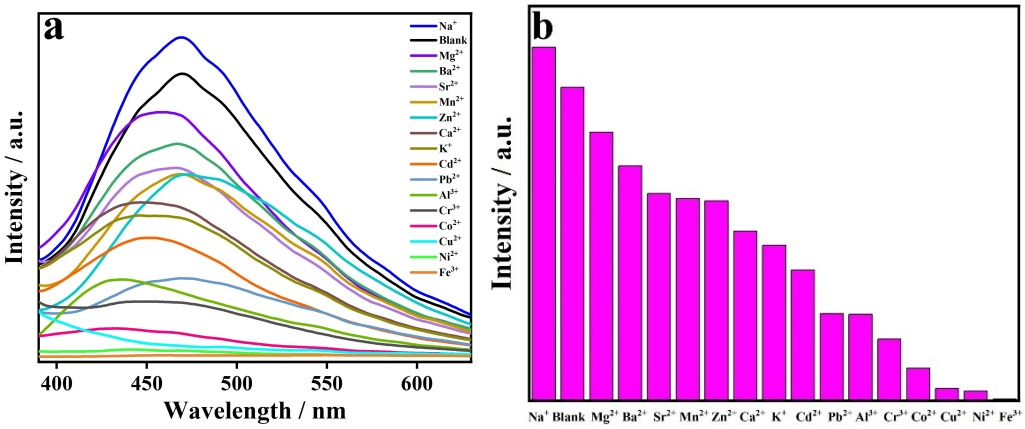

Figure 3. (**a**) Fluorescence spectra of CP **1** and (**b**) fluorescence intensities in different solutions of metal ions.

In order to evaluate the anti-interference ability of CP **1** for detecting Fe^{3+}, we explored the selective detection ability of CP **1** towards Fe^{3+} with competitive experiments (Figure 4), and further demonstrated that CP **1** can serve as a fluorescent turn-off sensor for detecting Fe^{3+}. The fluorescence response of CP **1** towards Fe^{3+} was investigated in the presence of interfering metal ions. A 1.5 mL Fe^{3+} solution (0.01 M) was slowly dripped into a suspension of the powder sample of CP **1** with 0.01 M interfering metal ions (Na^+, Mg^{2+}, Ba^{2+}, Sr^{2+}, Mn^{2+}, Zn^{2+}, Ca^{2+}, K^+, Cd^{2+}, Pb^{2+}, Al^{3+}, Cr^{3+}, Co^{2+}, Cu^{2+}, and Ni^{2+}), respectively. The fluorescence intensities of CP **1** decreased with a significant fluorescent turn-off effect after adding Fe^{3+}. The measured result indicates that CP **1** can selectively sense Fe^{3+} without interference from other metal ions.

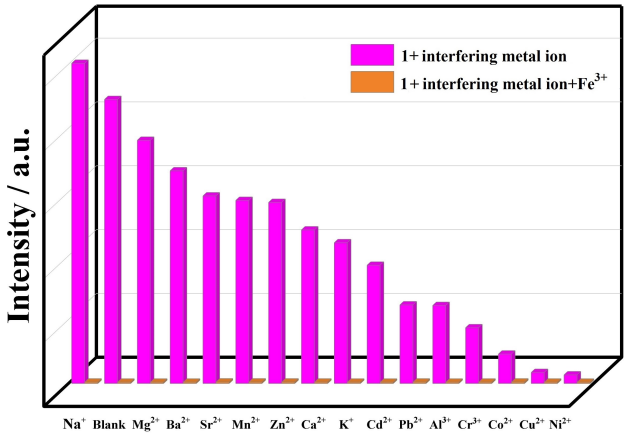

Figure 4. Fluorescence intensities of CP **1** in solutions with different interfering metal ions before and after addition of Fe^{3+}.

In order to further evaluate the detection sensitivity of CP **1** toward Fe^{3+} in detail, a titration experiment of quantitative fluorescence quenching was performed at the excitation wavelength of 334 nm (Figure 5a). With the addition of Fe^{3+}, the fluorescence quenching efficiency sequentially increased. The relationship between the concentration of Fe^{3+} and the fluorescence intensity of the suspension of powder sample of CP **1** can be analyzed with the Stern–Volmer equation: $I_0/I = K_{sv}[M] + 1$ in the range of low concentration, where I_0 and I are fluorescence intensities of the suspension of powder sample of CP **1** before and after the addition of Fe^{3+}, respectively, K_{sv} is the slope of the linear curve (quenching coefficient) and [M] is the molar concentration of Fe^{3+} (Figure 5b). The result indicates that the relationship conforms to the linear equation of $I_0/I = 0.123[Fe^{3+}] + 0.966$ with the linear correlation (R_2) of 0.990 and K_{sv} of 1.23×10^4 M^{-1}. Meanwhile, the LOD of CP **1** toward Fe^{3+} was further calculated to be 3.66×10^{-6} M by using the equation of LOD = $3\sigma/K_{sv}$, where σ is the standard deviation. We performed 11 consecutive measurements on the blank sample of CP **1** to obtain 11 fluorescence intensity values, and then calculated the σ value to be 0.015 [28].

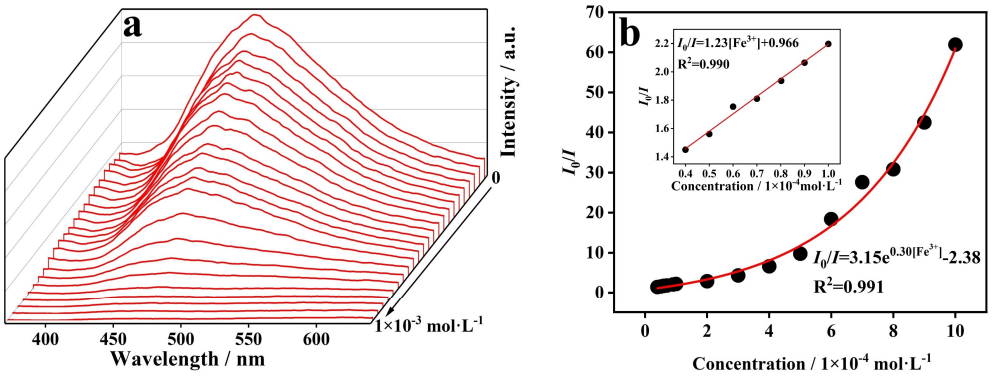

Figure 5. (**a**) Fluorescence responses of CP **1** in solutions with different concentrations of Fe^{3+} and (**b**) Stern–Volmer plot.

As the recyclability of CP **1** for sensing of Fe^{3+} can increase its potential application, recycling experiments were performed (Figure 6). After the first quenching induced by Fe^{3+}, it was regenerated by centrifugation and washing several times with deionized water, and its fluorescence quenching effect towards Fe^{3+} was examined again. The result revealed that the fluorescence intensity and quenching efficiency of CP **1** remained almost unchanged through at least three cycles of use, which indicates that CP **1** can be reused for detecting Fe^{3+} in water.

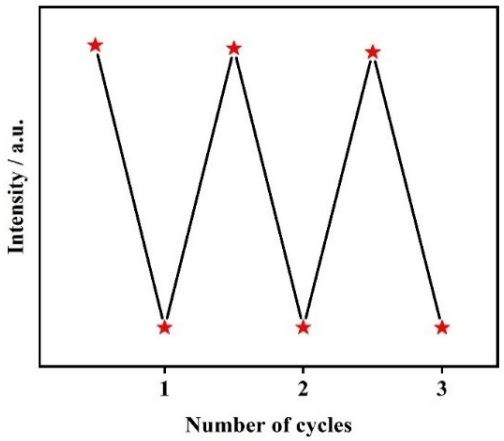

Figure 6. Recyclability of CP **1** for sensing of Fe^{3+}.

2.6. Mechanism of Fluorescence Response to Fe^{3+}

In order to investigate the mechanism of fluorescence quenching of CP **1** induced by Fe^{3+}, further investigations were conducted. After immersion in a solution of Fe^{3+} for 12 h, XRD measurement of the sample of CP **1** was performed (Figure 7a). A similar comparison of PXRD patterns revealed that the crystalline framework of CP **1** was not destroyed. The substitution of the central metal ion of CP **1** with the added Fe^{3+} will take a long time; however, the fluorescence of CP **1** is quenched relatively quickly by Fe^{3+}. Therefore, ion substitution is not the main reason for fluorescence quenching. The IR spectrum of the sample of CP **1** after immersion in Fe^{3+} solution essentially matched that of the pristine sample of CP **1**, indicating the non-coordination of N, O donors of functional groups in CP **1** with metal ions added (Figure S4). There was an overlap between the fluorescence emission band of CP **1** (λ_{ex} = 292 nm) and the UV-Vis absorption spectrum of Fe^{3+} (Figure 7b), which indicates that fluorescence resonance energy transfer occurs in the sensing process. In addition, the UV-Vis absorption spectrum of Fe^{3+} presented large overlap with the excitation band of CP **1** (λ_{em} = 390 nm) (Figure 7b), which indicated that the competitive absorption might be the main cause of fluorescence quenching of CP **1** by Fe^{3+}. In summary, based on the above results, the plausible mechanism of the quenching phenomenon can be attributed to the combined effect of resonance energy transfer and competitive energy absorption [28].

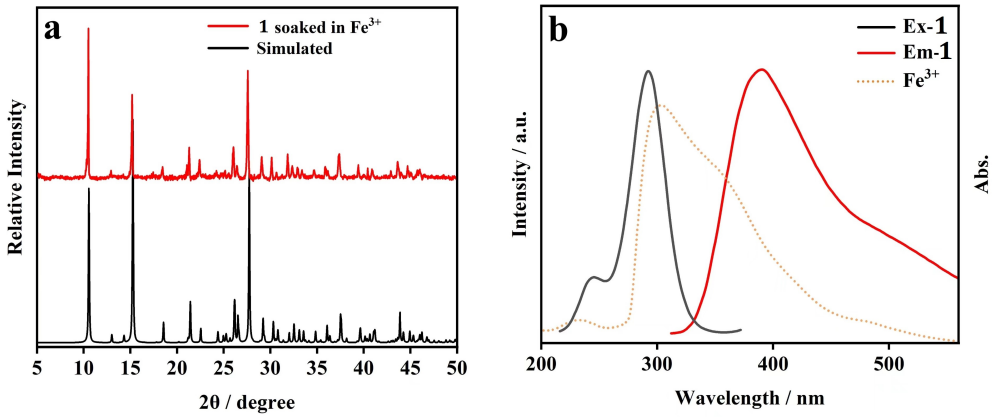

Figure 7. (**a**) PXRD pattern of CP **1** soaked in Fe^{3+} solution; (**b**) UV-Vis absorption spectrum of Fe^{3+}, fluorescence excitation and emission spectra of CP **1**.

2.7. Selective Sensing of $Cr_2O_7^{2-}$ and MnO_4^-

Industrial wastewater is usually composed of coexisting metal cations and inorganic anions, and thus, its analysis poses multiple challenges. Sensing measurements were

further performed at the excitation wavelength of 334 nm to explore the fluorescence responses of CP **1** to different inorganic anions (Figure 8a). A powder sample of CP **1** was ultrasonically dispersed in 0.01 M aqueous solutions of various potassium salts KM_x (M = NO_3^-, CO_3^{2-}, PO_4^{3-}, $H_2PO_4^-$, F^-, Cl^-, SO_4^{2-}, Br^-, $Cr_2O_7^{2-}$ and MnO_4^-), generating a suspension solution, respectively. It was found that inorganic anions induced different fluorescence responses on CP **1** (Figure 8b), especially $Cr_2O_7^{2-}$ and MnO_4^-, which could cause obvious fluorescent turn-off effects with quenching efficiencies of 99.4% and 99.5%, respectively. The results indicate that $Cr_2O_7^{2-}$ and MnO_4^- can be detected by CP **1** in aqueous solution. In addition, interference experiments were performed to detect $Cr_2O_7^{2-}$ and MnO_4^- in the presence of other inorganic anions, respectively (Figure 9). The fluorescence quenching intensity of CP **1** towards $Cr_2O_7^{2-}$ and MnO_4^- remained constant as the interfering anion was changed, respectively. It was evident that the fluorescent turn-off effects of $Cr_2O_7^{2-}$ and MnO_4^- on CP **1** were almost unaffected by the interfering inorganic anions, respectively.

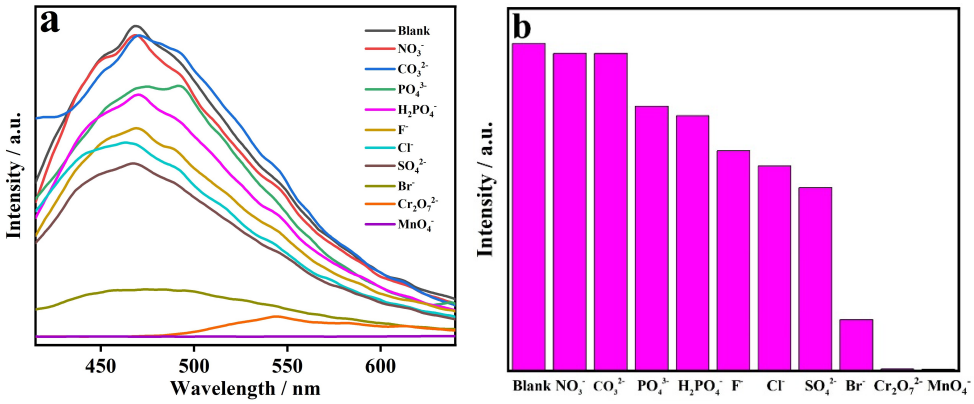

Figure 8. (**a**) Fluorescence spectra and (**b**) fluorescence intensities of CP **1** in different anionic solutions.

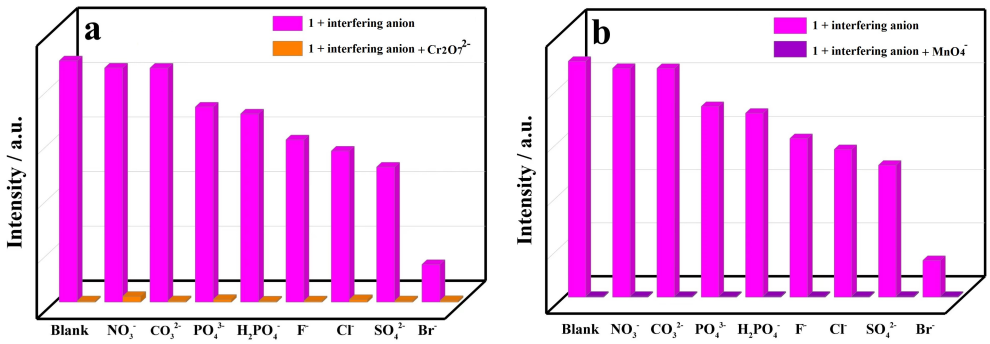

Figure 9. Fluorescence intensities of CP **1** in solutions with different interfering anions before and after addition of (**a**) $Cr_2O_7^{2-}$ and (**b**) MnO_4^-.

A titration experiment showed that the fluorescence intensity of CP **1** was gradually quenched at the excitation wavelength of 334 nm with the addition of $Cr_2O_7^{2-}$ and MnO_4^-, respectively (Figures 10 and 11). Moreover, the K_{sv} curves of $Cr_2O_7^{2-}$ and MnO_4^- showed good linear correlation, while the K_{sv} values for $Cr_2O_7^{2-}$ and MnO_4^- were 1.89×10^3 M^{-1} and 1.53×10^4 M^{-1}, respectively. Meanwhile, the LODs of $Cr_2O_7^{2-}$ and MnO_4^- were 2.38×10^{-5} and 2.94×10^{-6} M, respectively. The experimental results indicate that CP **1** can sensitively detect $Cr_2O_7^{2-}$ and MnO_4^- in water.

To evaluate the recyclability of CP **1** as a fluorescent sensor, the fluorescence of CP **1** was repeatedly quenched by $Cr_2O_7^{2-}$ and MnO_4^-, respectively (Figure 12). After each quenching, the powder sample of CP **1** was recovered through centrifugation, water washing and drying. The experimental results indicated that the fluorescent intensity of CP

1 can almost be restored after exposure to $Cr_2O_7^{2-}$ through at least four cycles; furthermore, the fluorescence quenching efficiency also remains unchanged, indicating that CP **1** has good recyclability for detecting $Cr_2O_7^{2-}$. However, the fluorescent intensity of CP **1** could not be restored for sensing of MnO_4^-, revealing its poor reversibility.

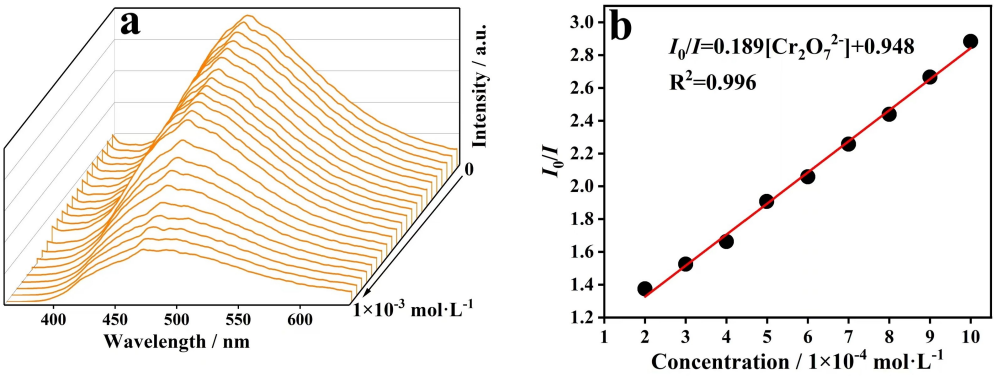

Figure 10. (**a**) Fluorescence responses of CP **1** in solutions with different concentrations of $Cr_2O_7^{2-}$ and (**b**) Stern–Volmer plot.

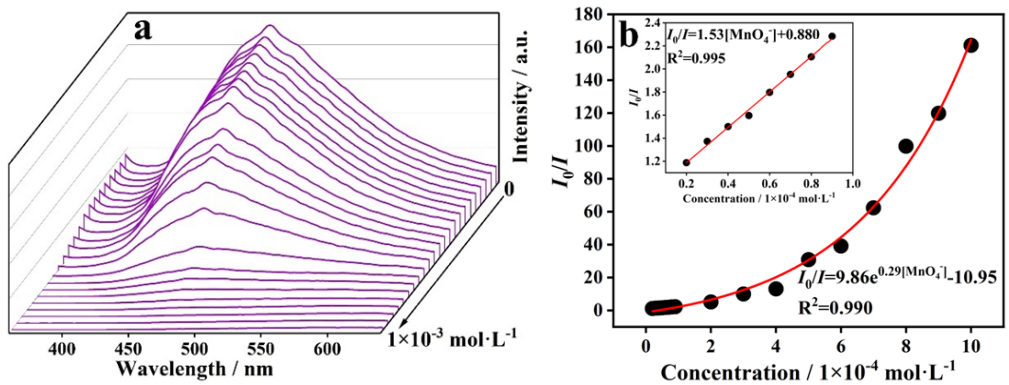

Figure 11. (**a**) Fluorescence responses of CP **1** in solutions with different concentrations of MnO_4^- and (**b**) Stern–Volmer plot.

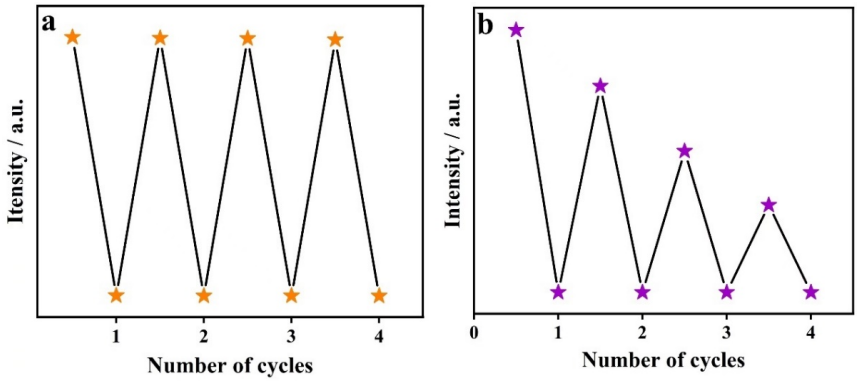

Figure 12. Cyclic experiments using CP **1** for detection of (**a**) $Cr_2O_7^{2-}$ and (**b**) MnO_4^-.

2.8. Mechanism of Fluorescence Response to $Cr_2O_7^{2-}$/MnO_4^-

In order to elucidate the mechanism of the fluorescence quenching of CP **1** induced by $Cr_2O_7^{2-}$/MnO_4^-, additional measurements were performed. The PXRD pattern of a sample of CP **1** immersed in the solution of $Cr_2O_7^{2-}$/MnO_4^- was consistent with the simulated one (Figure 13a), indicating that the fluorescence quenching was not caused by the collapse of the structure. The IR spectrum of the sample of CP **1** treated by the solution of $Cr_2O_7^{2-}$/MnO_4^- essentially matched with that of the pristine sample, indicating that

there was no weak interaction between CP **1** and the inorganic anions added (Figure S4). In addition, the UV-Vis absorption spectra of $Cr_2O_7^{2-}$/MnO_4^- overlapped the emission band of CP **1** (λ_{ex} = 292 nm) (Figure 13b), which indicated that the fluorescence quenching caused by $Cr_2O_7^{2-}$/MnO_4^- could be attributed to the resonance energy transfer. Moreover, a partial overlap existed between the absorption spectra of $Cr_2O_7^{2-}$/MnO_4^- and the excitation band of CP **1** (λ_{em} = 390 nm) (Figure 13b), which hindered the absorption of CP **1** and caused photoluminescence attenuation. Therefore, there is clear evidence for the competitive adsorption between each analyte and CP **1**. In summary, the fluorescence quenching mechanism of $Cr_2O_7^{2-}$/MnO_4^- on CP **1** is mainly attributed to the resonance energy transfer, as well as the competitive energy absorption [28].

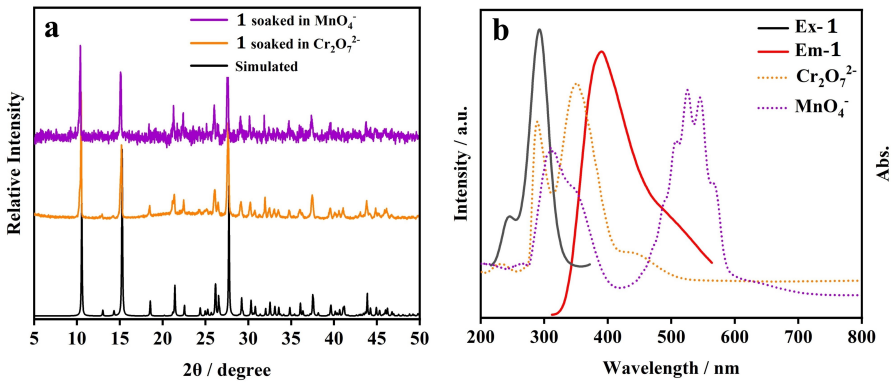

Figure 13. (**a**) PXRD patterns of CP **1** soaked in $Cr_2O_7^{2-}$ and MnO_4^- solution, respectively; (**b**) UV-Vis absorption spectra of $Cr_2O_7^{2-}$ and MnO_4^-, fluorescence excitation and emission spectra of CP **1**.

2.9. Comparison with Other, Related Sensors

Zn(II) CPs have been proven to be excellent sensing materials for metal cations and inorganic anions, etc. Some of them can only be utilized for the detection of a single analyte. For instance, a 2D Zn(II) CP $[Zn(4\text{-}PP)(1,4\text{-}BDC)\cdot(H_2O)]_n$ (1,4-PP = 4-(1H-pyrazol-3-yl)pyridine, 1,4-H_2BDC = 1,4-benzenedicarboxylic acid) synthesized under hydrothermal conditions exhibits selective and sensitive detection of Fe^{3+} in water medium [29]. However, the title Zn(II) CP displays multi-functional fluorescence responses towards Fe^{3+}, $Cr_2O_7^{2-}$ and MnO_4^-. The title CP was constructed by atyha$^-$ anions and Zn cations, and shows excellent sensing performances towards Fe^{3+}, $Cr_2O_7^{2-}$ and MnO_4^-, which are mainly due to the fluorescent turn-off effect. According to relevant reports in the literatures, it can be seen that these are comparable to or even better than those of other Zn(II) CPs [30–34]. Zhang et al. designed and prepared a Zn(II) CP as a dual-responsive luminescent sensor for Fe^{3+} and MnO_4^- in water, with LODs of 5.0×10^{-6} M and 8.86×10^{-6} M, respectively [30]. Another Zn-MOF with a 1D chain structure was confirmed as a multi-functional luminescence sensor for the detection of Fe^{3+} and $Cr_2O_7^{2-}$ in water through fluorescent quenching, and the LODs were 1.172×10^{-5} M and 2.465×10^{-4} M, respectively [31].

3. Experimental Section

3.1. Materials and Methods

All reagents and solvents were of reagent grade and purchased from Shanghai Aladdin Biochemical Technology Co., Ltd. Elemental analysis was performed with a Perkin-Elmer 240CHN analyzer (Perkin-Elmer Corporation, Norwalk CT, USA). FT-infrared spectra were collected by a Magna FT-IR 750 spectrometer (Nicolet, Tokyo, Japan) in the range of 4000 cm^{-1}–400 cm^{-1} (KBr pellet). Thermogravimetric data were collected on a NETZSCH STA 449C (Netzsch Corporation, Bavaria, Germany) unit between 25 °C and 900 °C with a heating rate of 10 °C·min^{-1} under a nitrogen atmosphere, with an Al_2O_3 crucible used to hold the solid sample. Fluorescence excitation and emission spectra were measured by a Perkin-Elmer LS55 fluorescence spectrophotometer (Perkin-Elmer Corporation, Norwalk,

CT, USA) using a 75W Xenon arc-lamp and an R928 photomultiplier tube as a detector for solid samples. Emission intensity measurements were carried out using the adapter and holder supplied by the manufacturer of thespectrophotometer. Excitation and emission spectra were corrected for the instrumental response. UV-Vis absorption spectra were measured by a UV-1800 spectrophotometer (ShiMadzu Corporation, Kyoto, Japan). Powder X-ray diffraction (PXRD) patterns were recorded on a Bruker D8 Advanced XRD diffractometer (Bruker, Rheinstetten, Germany) with Cu-K_α monochromator.

3.2. Synthesis of CP ***1***

A mixture of Hatyha ligand (0.037 g, 0.2 mmol) and $ZnCl_2$ (0.014 g, 0.1 mmol) in deionized water (20 mL), with its pH value adjusted to about 5 with NaOH (0.1 M) solution, was transferred to a 25 mL Teflon-lined autoclave and heated at 120 °C for 48 h. After cooling to room temperature, colorless blocked crystals of **1** were collected with a yield of 58% based on Zn(II). Elemental analysis (%) found: C, 27.46; H, 1.92; N, 19.26. Calcd for $C_{10}H_8N_6O_6S_2Zn$: C, 27.42; H, 1.83; N, 19.19%. IR (KBr, cm^{-1}): 3414, 3269 (ν_{NH2}), 3124($\nu_{O\text{-}H}$), 1632, 1347(ν_{COO^-}), 1512, 1424($\nu_{C=C,\,C=N}$), 1194, 1083, 1028($\nu_{C\text{-}O}$), 800($\delta_{C\text{-}H}$), 726, 641($\nu_{C\text{-}S}$), 535($\nu_{M\text{-}N}$) (Figure S4).

3.3. X-ray Crystallography

Single-crystal X-ray diffraction data for CP **1** were recorded using a Bruker D8 VENTURE diffractometer with graphite-monochromatized Mo-K_α radiation (λ = 0.71073 Å) by φ-ω scan mode. The structure was solved by direct methods and refined by full-matrix least-squares techniques using the SHELXS and SHELXL programs, respectively [35,36]. For CP **1**, crystallographic data and structure refinement details are summarized in Table 1. Selected bond lengths and bond angles are given in Table 2.

4. Conclusions

In conclusion, a novel 2D Zn-based coordination polymer was hydrothermally synthesized by introducing Hatyha ligand. The atyha$^-$ linkers adopted the carboxylate, thiazole and oxime groups to bridge with Zn^{2+}, generating a 2D framework with Schläfli symbol $\{4^4{\cdot}6^2\}$ topology. Notably, CP **1** displays strong fluorescence emission, which is derived from intraligand transition. It exhibits high structural stabilities towards aqueous solutions. It was found that CP **1** could not only detect Fe^{3+} and $Cr_2O_7^{2-}$ with high selectivity, sensitivity and recyclability, but also serve as an excellent candidate for the selective and sensitive sensing of MnO_4^-, indicating low LODs of 3.66×10^{-6}, 2.38×10^{-5} and 2.94×10^{-6} M, respectively. The mechanism of the fluorescence turn-off sensing can be attributed to the synergistic effect of resonance energy transfer and competitive energy absorption.

Supplementary Materials: The following supporting information can be downloaded at: https://www.mdpi.com/article/10.3390/molecules29122943/s1, Figure S1: TGA curve of CP **1**; Figure S2: Measured and simulated PXRD patterns of CP **1**; Figure S3: PXRD patterns of CP **1** soaked in water for 12 h and 7 d; Figure S4: IR spectra of sample of CP **1**, as well as after immersion in Fe^{3+}, $Cr_2O_7^{2-}$ and MnO_4^- solutions, Table S1: Hydrogen bond lengths (Å) and bond angles (°) for CP **1**.

Author Contributions: Conceptualization, L.G.; methodology, L.G.; software, M.Z.; validation, Y.L., D.Z., X.H. and Y.G.; formal analysis, M.Z.; investigation, M.Z., L.G. and Y.W.; resources, L.G.; data curation, L.G.; writing—original draft preparation, Y.L. and M.Z.; writing—review and editing, L.G. and Y.W.; supervision, L.G.; project administration, Y.W. All authors have read and agreed to the published version of the manuscript.

Funding: This research was funded by Basic Scientific Research Project of Universities from Liaoning Provincial Education Department, grant number LJKMZ20220738.

Data Availability Statement: The data presented in this study are available on request from the corresponding author.

Conflicts of Interest: The authors declare no conflicts of interest.

References

1. Zhao, X.Y.; Wu, J.F.; Tian, W. Terbium(III)-based coordination polymer with millimeter-size single crystals and high selectivity and sensitivity for folic acid. *CrystEngComm* **2023**, *25*, 945–952. [CrossRef]
2. Liu, L.J.; Zhu, H.; Han, C.; Cui, G.H.; Fu, L.S. Luminescent detecting of Fe^{3+} and $Cr_2O_7^{2-}$ ions by three ternary 2D coordination polymers. *Polyhedron* **2021**, *198*, 115074. [CrossRef]
3. Zhou, H.C.; Long, J.R.; Yaghi, O.M. Introduction to metal-organic frameworks. *Chem. Rev.* **2012**, *112*, 673–674. [CrossRef] [PubMed]
4. Barnett, B.R.; Gonzalez, M.I.; Long, J.R. Recent progress towards light hydrocarbon separations using metal-organic frameworks. *Trends Chem.* **2019**, *1*, 159–171. [CrossRef]
5. Zhao, Q.; Li, Q.Y.; Li, J. Structures, fluorescence and magnetism of a series of coordination polymers driven by a tricarboxypyridine ligand. *CrystEngComm* **2022**, *24*, 6751–6761. [CrossRef]
6. Andac, O.; Gorduk, S.; Yilmaz, H. Synthesis, characterization and H_2 adsorption performances of polymeric Co(II) and Ni(II) complexes of pyrazine-2,3-dicarboxylic acid and 1-vinylimidazole. *J. Iran. Chem. Soc.* **2018**, *15*, 1699–1708. [CrossRef]
7. Liu, H.J.; Yi, R.; Chen, D.M.; Huang, C.; Zhu, B.X. Self-assembly by tridentate or bidentate ligand: Synthesis and vapor adsorption properties of Cu(II), Zn(II), Hg(II) and Cd(II) complexes derived from a bis(pyridylhydrazone) compound. *Molecules* **2021**, *26*, 109. [CrossRef] [PubMed]
8. Kuwamura, N.; Konno, T. Heterometallic coordination polymers as heterogeneous electrocatalysts. *Inorg. Chem. Front.* **2021**, *8*, 2634–2649. [CrossRef]
9. Sun, Y.Q.; Cheng, Y.; Yin, X.B. Dual-ligand lanthanide metal-organic framework for sensitive ratiometric fluorescence detection of hypochlorous acid. *Anal. Chem.* **2021**, *93*, 3559–3566. [CrossRef]
10. Zhang, D.C.; Li, X. A Zn(II) complex with large channels based on 3′-nitro-biphenyl-3,5,4′-tricarboxylic acid: Synthesis, crystal structure, fluorescence sensing of ATP, ADP, GTP, and UTP in aqueous solution and drug delivery. *CrystEngComm* **2017**, *19*, 6673–6680. [CrossRef]
11. Wen, M.Y.; Ren, L.; Cui, G.H. Two Co(II) complexes containing pyridylbenzimidazole ligands as chemosensors for the sensing of levofloxacin, acetylacetone, and Ni^{2+} with high selectivity and sensitivity. *CrystEngComm* **2021**, *23*, 8563–8571. [CrossRef]
12. Xu, N.; Zhang, Q.H.; Zhang, G.A. A carbazole-functionalized metal-organic framework for efficient detection of antibiotics, pesticides and nitroaromatic compounds. *Dalton Trans.* **2019**, *48*, 2683–2691. [CrossRef] [PubMed]
13. Arici, M. Multifunctional luminescent coordination polymers based on tricarboxylic acid for the detection of 2,4-dinitrophenol and iron(III) and aluminum(III) ions. *New J. Chem.* **2019**, *43*, 3690–3697. [CrossRef]
14. Goshisht, M.K.; Tripathi, N. Fluorescence-based sensors as an emerging tool for anion detection: Mechanism, sensory materials and applications. *J. Mater. Chem. C* **2021**, *9*, 9820–9850. [CrossRef]
15. Jana, A.K.; Natarajan, S. Fluorescent metal-organic frameworks for selective sensing of toxic cations (Tl^{3+}, Hg^{2+}) and highly oxidizing anions [$(CrO_4)^{2-}$, $(Cr_2O_7)^{2-}$, $(MnO_4)^{-}$]. *ChemPlusChem* **2017**, *82*, 1153–1163. [CrossRef] [PubMed]
16. Rao, P.C.; Mandal, S. Europium-based metal-organic framework as a dual luminescence sensor for the selective detection of the phosphate anion and Fe^{3+} ion in aqueous media. *Inorg. Chem.* **2018**, *57*, 11855–11858.
17. Alexandrov, E.V.; Shevchenko, A.P.; Nekrasova, N.A.; Blatov, V.A. Topological methods for analysis and design of coordination polymers. *Russ. Chem. Rev.* **2022**, *91*, RCR5032. [CrossRef]
18. Sokolov, A.V.; Vologzhanina, A.V.; Sudakova, T.V.; Popova, Y.V.; Alexandrov, E.V. Design and synthesis of coordination polymers with Cu(II) and heterocyclic *N*-oxides. *CrystEngComm* **2022**, *24*, 2505–2515. [CrossRef]
19. Tran, M.; Kline, K.; Qin, Y.; Shen, Y.X.; Green, M.D.; Tongay, S. 2D coordination polymers: Design guidelines and materials perspective. *Appl. Phys. Rev.* **2019**, *6*, 041311. [CrossRef]
20. Fan, Y.R.; Li, H.B.; Ji, Z.Y.; Liu, J.Y.; Wu, M.Y. Syntheses, structures and photoluminescence of three Zn(II) coordination polymers based on N-containing heterocyclic ligand and varied auxiliary ligands. *Inorg. Chem. Commun.* **2019**, *102*, 229–232. [CrossRef]
21. Li, J.D.; Bai, C.; Hu, H.M.; Yang, Z.H.; Xue, G.L. Solvothermal syntheses, crystal structures and luminescence properties of Zn(II) coordination compounds based on imidazophenanthroline carboxylate derivative ligand. *J. Solid State Chem.* **2019**, *227*, 1–8. [CrossRef]
22. Wang, Y.N.; Xu, H.; Wang, S.D.; Chang, X.P.; Wang, Y.T.; Qiu, Q.C.; Bai, J.T.; Mo, Y.; Feng, W.Y.; Zhang, M.H.; et al. Efficient antibiotics, small organic molecules and inorganic anions detection with a fluorescent Ni(II) coordination polymer based multiple sensor system. *J. Mol. Struct.* **2024**, *1296*, 136829. [CrossRef]
23. Saini, K.; Singh, J.; Malik, S.; Saharan, Y.; Goyat, R.; Umar, A.; Akbar, S.; Ibrahim, A.A.; Baskoutas, S. Metal-Organic Frameworks: A promising solution for efficient removal of heavy metal ions and organic pollutants from industrial wastewater. *J. Mol. Liquids* **2024**, *399*, 124365. [CrossRef]
24. Devi, M.K.; Yaashikaa, P.R.; Kumar, P.S.; Oviyapriya, M.; Varshika, V.; Rangasamy, G. Recent advances in carbon-based nanomaterials for the treatment of toxic inorganic pollutants in wastewater. *New J. Chem.* **2023**, *47*, 7655–7667. [CrossRef]
25. Agarwal, R.A. One Dimensional Coordination Polymer of Zn(II) for Developing Multifunctional Nanoparticles. *Sci. Rep.* **2017**, *7*, 13212. [CrossRef] [PubMed]

26. Blatov, V.A.; Shevchenko, A.P.; Proserpio, D.M. Applied topological analysis of crystal structures with the program package ToposPro. *Cryst. Growth Des.* **2014**, *14*, 3576–3586. [CrossRef]
27. Cao, H.Y.; Liu, Q.Y.; Li, L.Q.; Wang, Y.L.; Chen, L.L.; Yao, Y. Two cadmium coordination compounds with 5-sulfonyl-1,2,4-benzenetricarboxylate ligand: Syntheses, structures, and photoluminescence. *Z. Anorg. Allg. Chem.* **2014**, *640*, 1420–1425. [CrossRef]
28. Zhu, C.Y.; Wang, C.L.; Chen, L.; Gao, W.; Li, P.; Zhang, X.M. A water-stable Zn(II) coordination polymer for a high sensitivity detection of Fe^{3+} and 2,4,6-trinitrophenol. *J. Solid State Chem.* **2022**, *310*, 123079. [CrossRef]
29. Liu, N.; Xing, G.E.; Huang, X.X.; Guo, J. A new Zn(II) coordination polymer constructed from 4-(1H-pyrazol-3-yl)pyridine as fluorescent sensor for Fe^{3+}. *Chin. J. Struct. Chem.* **2019**, *38*, 660–666.
30. Zhang, X.Q.; Chen, F.M.; Wen, Q.; Zhou, C.C.; He, X.; Li, Y.; Liu, H.F. Zn-based coordination polymers with tricarboxylic acid ligand: Fluorescence sensor toward Fe^{3+} and MnO_4^-. *J. Struct. Chem.* **2022**, *1252*, 132183. [CrossRef]
31. Wang, Y.N.; Ma, Y.L.; Zhang, S.S.; Li, S.F.; Du, L.; Zhao, Q.H. A multifunctional Zn-based coordination polymer showing luminescence detection toward multiple pollutants in water. *Inorg. Chem. Commun.* **2021**, *126*, 108476. [CrossRef]
32. Wang, Y.; Liu, Y.; Zhang, X.S.; Luan, J.; Yang, A.A.; Li, W.Z. Effect of secondary bis-pyridine-bis-amide ligand on the construction of Zn-based coordination polymers and the enhancement of ultrasensitive luminescent sensing properties. *J. Solid State Chem.* **2022**, *315*, 123516. [CrossRef]
33. Liu, G.C.; Han, S.W.; Gao, Y.; Xu, N.; Wang, X.L.; Chen, B.K. Multifunctional fluorescence responses of phenylamide-bridged d^{10} coordination polymers structurally regulated by dicarboxylates and metal ions. *CrystEngComm* **2020**, *22*, 7952–7961. [CrossRef]
34. Chai, Y.H.; Liu, X.Y.; Cui, Z.Y.; Zhao, Y.; Ma, L.F.; Zhao, B.T. Design and syntheses of two luminescent metal-organic frameworks for detecting nitro-antibiotic, Fe^{3+} and $Cr_2O_7^{2-}$. *J. Solid State Chem.* **2022**, *312*, 123211. [CrossRef]
35. Sheldrick, G.M. SHELXT-integrated space-group and crystal-structure determination. *Acta Crystallogr. Sect. A Found. Adv.* **2015**, *71*, 3–8. [CrossRef]
36. Sheldrick, G.M. Crystal structure refinement with SHELXL. *Acta Crystallogr. Sect. C Struct. Chem.* **2015**, *71*, 3–8. [CrossRef]